International Journal of Advanced Robotic Systems



# Design of a Knee Exoskeleton Using Foot Pressure and Knee Torque Sensors

Regular Paper

Jung-Hoon Kim[1], Myounghoon Shim[2], Dong Hyun Ahn[3], Byoung Jong Son[2], Suk-Young Kim[2], Deog Young Kim[4], Yoon Su Baek[2] and Baek-Kyu Cho[3]*

1 Construction Robot and Automation Laboratory, School of Civil and Environmental Engineering, Yonsei University, South Korea
2 School of Mechanical Engineering, Yonsei University, South Korea
3 Department of Mechanics and Design, Kookmin University, South Korea
4 Department and Research Institute of Rehabilitation Medicine, Yonsei University College of Medicine, South Korea
*Corresponding author(s) E-mail: swan0421@gmail.com

Received 30 December 2014; Accepted 18 April 2015

DOI: 10.5772/60782



## Abstract

This study presents the development of a modular knee exoskeleton system that supports the knee joints of hemiplegic patients. The device is designed to realize the polycentric motion of real human knees using a four-bar linkage and to minimize its total weight. In order to determine the user's intention, force-sensitive resistors (FSRs) in the user's insole, a torque sensor on the robot knee joint, and an encoder in the motor are used. The control algorithm is based on a finite state machine (FSM), where the force control, position control and virtual damping control are applied in each state. The proposed hardware design and algorithm are verified by performing experiments on the standing, walking and sitting motion controls while wearing the knee exoskeleton.

**Keywords** Exoskeleton Robot, Knee Assistive Device, Rehabilitation Robot, Foot Pressure Sensor, Walking Assistance Control

## 1. Introduction

Exoskeletons are wearable robots that are created to assist the human body or increase the muscular power of the wearer. In particular, a lower limb exoskeleton can assist rehabilitation training and walking in paraplegic or hemiplegic patients, and exoskeletons are dramatically expanding their market share in the rehabilitation business. Compared with previous assistance methods such as wheelchairs, which cannot move on non-flat surfaces like stairs, lower limb exoskeletons enable patients to move on any surface. The primary goal of lower limb rehabilitation robots is to assist patients to walk in order to regain a better gait and to reduce the therapist's work. Furthermore, from a psychological perspective, they can help strengthen a patient's willingness and sense of achievement during rehabilitation.

Much notable research about walking assistance exoskeletons for paraplegic patients has been reported, such as ReWalk, Hybrid Assistive Limb (HAL) and eLEGS. ReWalk, which was developed by Argo Medical Technologies Inc., and eLEGS, which was developed by Ekso

Bionics at Berkeley, are exoskeletons that assist the entire lower limb with a walking stick [1-3]. In addition, HAL, which was developed by Tsukuba University and Cyberdyne Inc., is another example of an exoskeleton that assists lower limbs [4]. Theses exoskeletons have electric motors or hydraulic actuators on the hip and/or knee joints to assist with power, and they have force, motion or bioelectrical sensors to determine the user's intentions.

In this paper, we only focus on the knee joint. Previous research on knee joint exoskeletons include an EMG-based knee exoskeleton from Berlin University [5] and a spring-attached knee exoskeleton from MIT [6, 7], among others. Tibion (Bionic Leg), developed by AlterG, has been commercialized and many patients have used it [8, 9]. Except for Tibion, knee exoskeletons have had limited commercialization due to their heaviness and low performance. Furthermore, many of the existing knee exoskeletons are constructed using a single-axis knee joint.

Regarding single-joint artificial orthotics, they have a simple hinge structure that can be constructed easily as well as having good durability. However, they can only control the swing phase and cannot control the stance phase sufficiently. Real human knee joints move with a polycentric motion, whereby the centre of rotation changes during the rotation [10]. Due to this characteristic, a single-joint exoskeleton cannot fully track the human knee-joint motion. Furthermore, loss of energy occurs as a result of this centre misalignment.

For a polycentric joint, the structure is complicated and its durability is lower than that of a single-axis joint. However, the instant centre of rotation (ICOR) changes during rotation, and this generates moments that help reduce the energy required from the wearer during walking [11, 12]. Furthermore, during the swing phase of the gait motion, the ICOR variation increases the foot clearance from the ground, thus providing more stable movement [13]. The Tibion passively follows the polycentric path of a human knee joint. In this research, the knee joint is designed to actively follow the polycentric path using a four-bar linkage structure.

Because hemiplegic patients cannot move like healthy people, it is difficult to determine their intentions. As such, we used an insole-type foot sensor and torque sensor, consisting of strain gauges attached to the frame and being designed to sense the weight shifting and motion intention. Finally, as a basic test for verifying the developed hardware and sensor system, control algorithms were designed to assist the normal gait in order to move from sitting to standing and to move from standing to sitting. The impedance and position controller are used alternately to control the robot.

This paper proposes a knee assistant exoskeleton robot system for people with weak knee muscular power and difficulty in walking or standing. In Section 2, the light-weight actuator module design, including the four-bar linkage, is presented. The electrical hardware and foot sensor specifications are described in Section 3, and the control algorithm for the entire system is presented and tested in Section 4. Finally, Section 5 concludes the paper.

## 2. Design of a Polycentric Knee Actuator Module

In prostheses, the characteristics of a polycentric knee joint have been realized using a four-bar linkage. Currently, a four-bar linkage is also used in assisting devices, and these linkages have had numerous research outcomes related to exoskeletons [14, 15]. However, the four-bar linkage that is used in assisting devices is used for different features than those that prostheses have. Because the four-bar linkage can provide a polycentric motion similar to that of a human knee joint, it can reduce the relative motion between the wearer and the assistive device. If the relative motion is not reduced, the resulting friction would scratch the user's skin and become a source of loose binding force. Therefore, four-bar linkages can minimize these problems and improve feeling when wearing the exoskeleton due to the similarity of its motion to human knee joints.

This research applied a four-bar linkage to the actuating module for a knee joint, and the linkage length was determined by referring to [14]. Furthermore, analyses were performed to estimate the output torque and speed, which changes depending upon the crank rotation of the four-bar linkage.

The driving part of an actuating module is composed of a motor and a gear reducer (Figure 1). The motor selected was the Kollmorgen 01810C (24 V), and the Harmonic Drive SHD model (100:1) was used for the gear reducer. Although the motor and gear reducer have large diameters, their small lengths can help to minimize the volume of the actuating module. The Robocube BL2408-SID (200 W) was selected for the motor driver, and the CUI incremental encoder was selected for position and velocity feedback. Finally, the continuous stall torque and maximum rotation speed were 42.9 Nm and 225.3 deg/s, respectively.

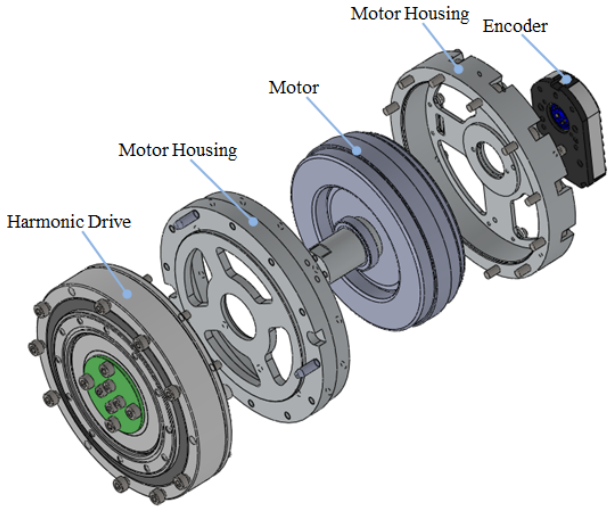


**Figure 1.** The actuating module for the knee exoskeleton

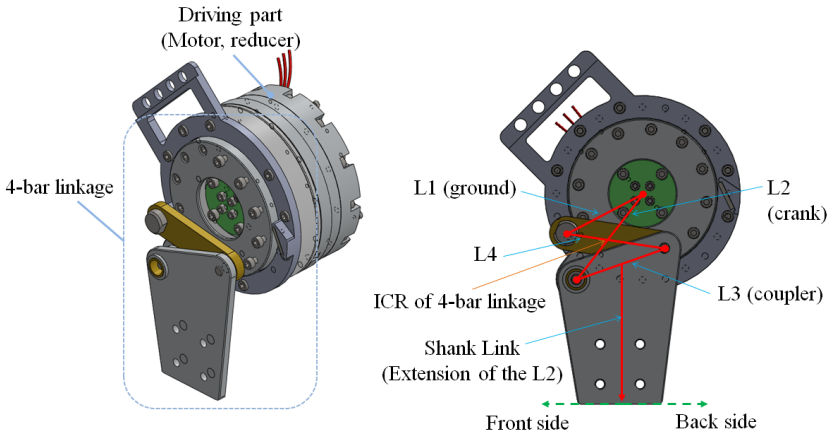


**Figure 2.** Four-bar linkage of the actuator module

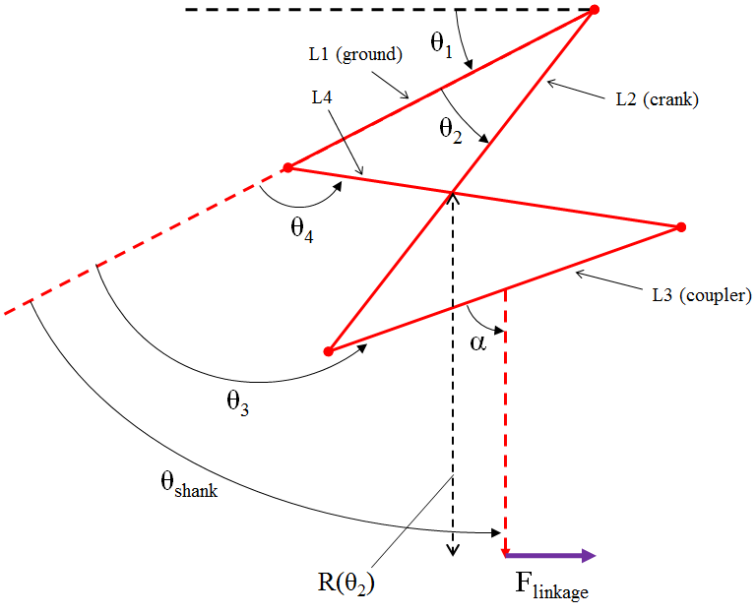


**Figure 3.** Four-bar linkage notation

While walking on level ground, the average peak knee extension moment is 40.5 Nm [16]. The angular speed cannot be fixed to a certain value because the rotation speed of the knee differs from person to person. However, for able-bodied subjects, it can be estimated to be 360~400 deg/s [17]. When the speed of the actuating module (225.3 deg/s) is too slow, it can disturb the wearer's walking motion. Therefore, the actuating module was designed with a focus on bringing its rotation speed to the required rotation speed of a human knee during level walking. Therefore, we designed the parameters of the four-bar linkage to satisfy the conditions required for the rotation speed. The four-bar linkage can modify the torque and speed characteristics of the actuating module. Their relationships are described in the next section.

In order to drive a four-bar linkage, the driving part was connected to a crank (L2) (Figures 2 and 3). As the crank rotated, the ICOR of the four-bar linkage's coupler (the same as the intersecting point of L2 and L4 in Figure 3) moved along a predefined path that was most similar to the ICOR of a human knee joint (Figure 4). The coupler of the four-bar linkage (L3) is connected to a user's shank, and it generates the shank motion. Because the system assists the wearer's shanks with polycentric motion, it is favourable in retaining the comfortableness and binding force between the wearer and system by reducing the friction.

Utilizing the four-bar linkage, the torque and rotation speed of the system can be controlled through the operation of the motor attached to the crank. In its initial state, the system generates a high speed and a low torque. As the rotating angle increases (as the wearer bends his/her knee), the speed is decreased while the torque is increased. This research's current actuating module generates a shank motion utilizing a coupler; thus, the output torque and

rotation speed of the module are changed with variations in the angles. The relationship between the coupler's rotational angle ($\theta_{shank}$) and the crank angle ($\theta_2$) can be calculated using equation (1) [18].

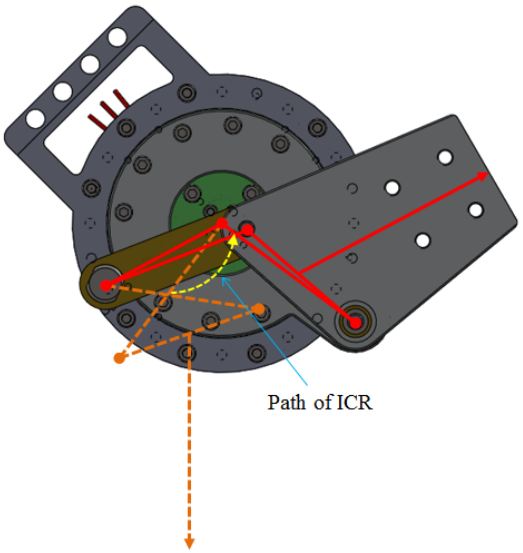


**Figure 4.** Path of the ICOR as the crank rotates

$$\theta_{shank} = \theta_3 - (180 - \alpha) = 2\arctan\left(\frac{-E + \sqrt{E^2 - 4DF}}{2D}\right) - (180 - \alpha) \quad (1)$$

where,

$$\alpha = 70.5 \text{ (design constants)}$$
$$D = \cos\theta_2 - K_1 + K_4\cos\theta_2 + K_5$$
$$E = -2\sin\theta_2,\ F = K_1 + (K_4 - 1)\cos\theta_2 + K_5$$
$$K_1 = \frac{L_1}{L_2},\ K_4 = \frac{L_1}{L_3},\ K_5 = \frac{{L_4}^2 - {L_1}^2 - {L_2}^2 - {L_3}^2}{2L_2L_3}$$

Furthermore, the final force ($F_{linkage}$) generated by the coupler can be calculated using equation (2) when the continuous stall torque ($T_{motor}$) is applied to the crank. After the calculations, the force vector was rotated as $\theta_1$ (= 27.5°; design constant). Figure 5 presents the $F_{linkage}$ of the crank rotation that a coupler exerted on the shank.

$$F_{linkage} = f(T_{motor}, \theta_2)$$
$$= inv\begin{bmatrix} 1 & 0 & 1 & 0 & 0 & 0 & 0 & 0 & 0 \\ 0 & 1 & 0 & 1 & 0 & 0 & 0 & 0 & 0 \\ -R_{12y} & R_{12x} & -R_{32y} & R_{32x} & 0 & 0 & 0 & 0 & 0 \\ 0 & 0 & -1 & 0 & 1 & 0 & 0 & 0 & \cos\theta_F \\ 0 & 0 & 0 & -1 & 0 & 1 & 0 & 0 & \sin\theta_F \\ 0 & 0 & R_{23y} & -R_{23x} & -R_{43y} & R_{43x} & 0 & 0 & K \\ 0 & 0 & 0 & 0 & -1 & 0 & 1 & 0 & 0 \\ 0 & 0 & 0 & 0 & 0 & -1 & 0 & 1 & 0 \\ 0 & 0 & 0 & 0 & R_{34y} & -R_{34x} & -R_{14y} & R_{14x} & 0 \end{bmatrix}\begin{bmatrix} 0 \\ 0 \\ T_{motor} \\ 0 \\ 0 \\ 0 \\ 0 \\ 0 \\ 0 \end{bmatrix}$$

*where,*

$$\theta_F = \theta_3 - 180 + \alpha - 90,\ K = \left(RP_x\sin\theta_F - RP_y\cos\theta_F\right)$$
$$R_{12x} = \frac{L2}{2}\cos(\theta_2 + \pi),\ R_{12y} = \frac{L2}{2}\sin(\theta_2 + \pi)$$
$$R_{32x} = \frac{L2}{2}\cos(\theta_2),\ R_{32y} = \frac{L2}{2}\sin(\theta_2)$$
$$R_{23x} = \frac{L3}{2}\cos(\theta_3),\ R_{23y} = \frac{L3}{2}\sin(\theta_3) \quad (2)$$
$$R_{43x} = \frac{L3}{2}\cos(\theta_3 + \pi),\ R_{43y} = \frac{L3}{2}\sin(\theta_3 + \pi)$$
$$R_{34x} = \frac{L4}{2}\cos(\theta_4),\ R_{34y} = \frac{L4}{2}\sin(\theta_4)$$
$$R_{14x} = \frac{L4}{2}\cos(\theta_4 + \pi),\ R_{14y} = \frac{L4}{2}\sin(\theta_4 + \pi)$$

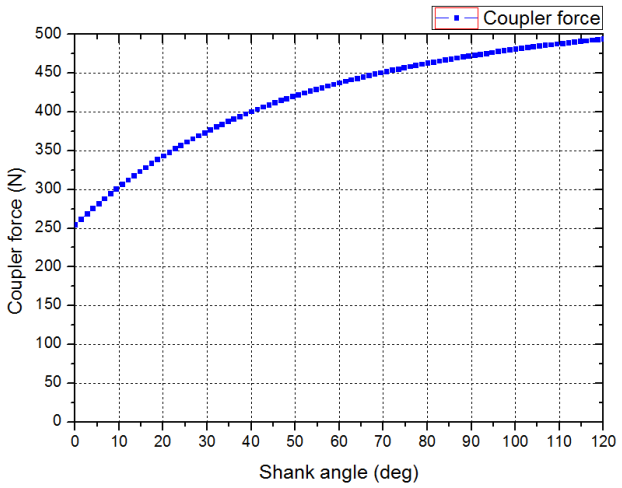


**Figure 5.** $F_{linkage}$ variation as the crank rotates

Additionally, the moment arm from the ICOR to the shank ($R(\theta_2)$) changes depending upon the crank angle. This change is illustrated in Figure 6, and its variation was less than 4% of the initial moment arm.

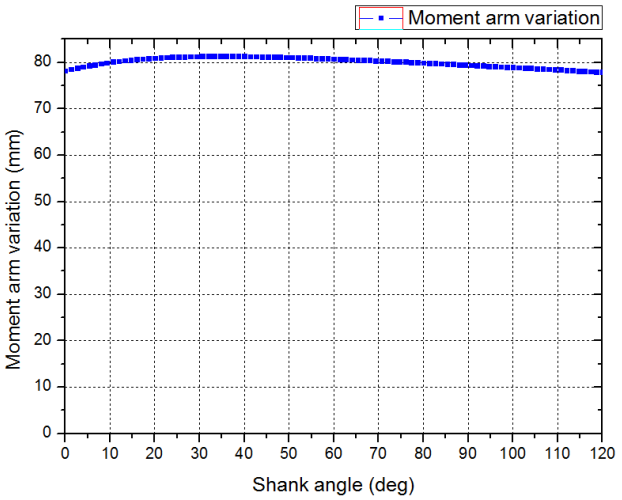


**Figure 6.** Variation of the moment arm $R(\theta_2)$

Finally, the output torque of the coupler ($T_{shank}$) can be estimated using the input torque of the crank ($T_{motor}$) and

moment arm. This relationship is described in equation (3) and is plotted in Figure 7.

$$T_{shank} = F_{linkage}\left(T_{motor}, \theta_2\right) \times R\left(\theta_2\right) \quad (3)$$

The rotation speed can be computed using P = Tw. Thus, the output speed was computed using a simulation (Figure 8).

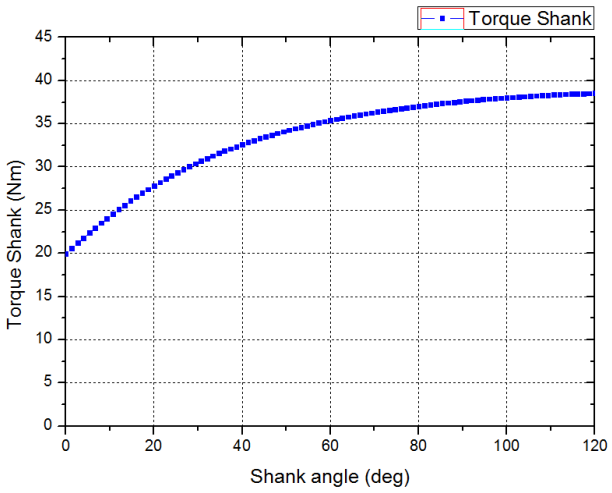


**Figure 7.** Variations of the output torque

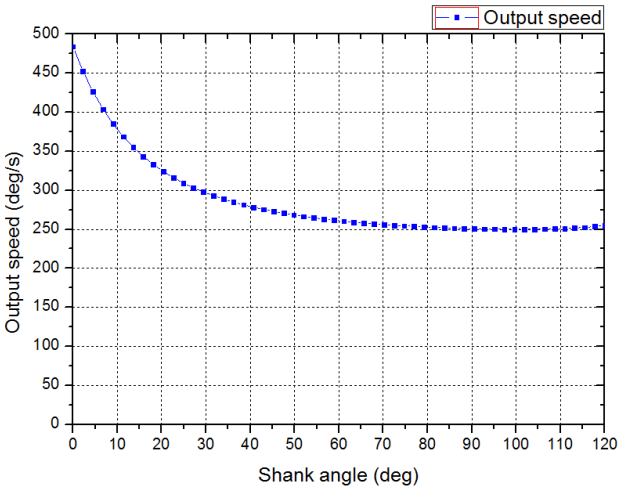


**Figure 8.** Variations of the output speed

As a result of these features, the actuating module can exert more torque on a user as the knee joint angle increases. In daily life, users need a significant amount of torque when they bend their knees, particularly when moving from sitting to standing, climbing stairs, and so on. Therefore, the output characteristics of the actuating module that exert a higher torque with the bending angle are appropriate in assisting these performances.

From the perspective of level walking, the human knee joint requires different torques and speeds according to the joint angle or walking phase. Furthermore, the actuating module can generate different torques and speeds according to its crank (L2) angle. Therefore, a comparison of the actuating module's torque and speed with clinical data of a knee joint engaged in walking motion was simulated.

In Figure 9, the comparison of the torque characteristics of the clinical data (black), the actuating module or four-bar linkage (red), and the single-axis joint (blue) are presented. The output torque of the single-axis fully satisfies the required human knee joint torque; that of the actuating module has slight dissatisfaction for 10~20% of the walking phase. However, the robot does not need to satisfy all required knee joint torques. Because the target users have hemiparesis, they can exert a slight knee torque that does not fully satisfy the required knee torque for walking.

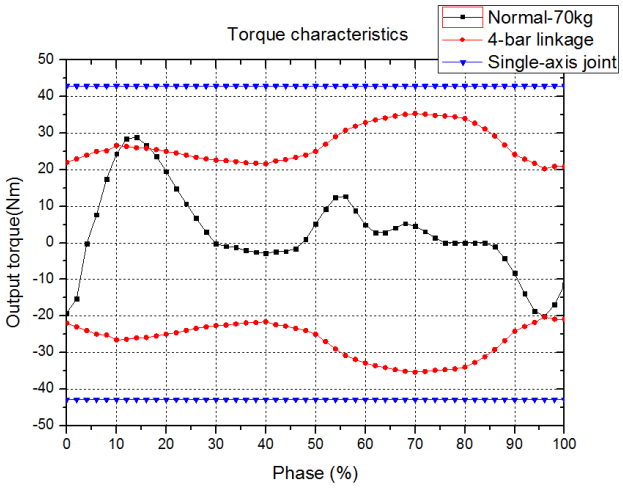


**Figure 9.** Comparison of torque characteristics: normal person (black), four-bar linkage (red), and single-axis joint (blue)

In Figure 10, the comparison of the speed characteristics of the clinical data (black), the actuating module or four-bar linkage (red), and the single-axis joint (blue) are presented. The output speed of the single-axis was unsatisfactory for 56~68% and 82~94% of the walking phase. On the other hand, the output speed of the actuating module was not satisfactory at 60~67% of the walking phase only.

Although the system does not 100% match its output to the walking speed of an able-bodied person, its performance is sufficient to assist the user's walking motion while satisfying the ICOR of a knee joint.

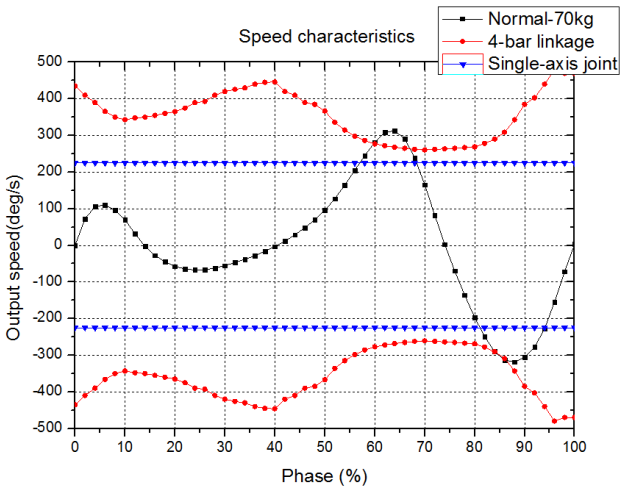


**Figure 10.** Comparison of speed characteristics: normal person (black), four-bar linkage (red) and single-axis joint (blue)

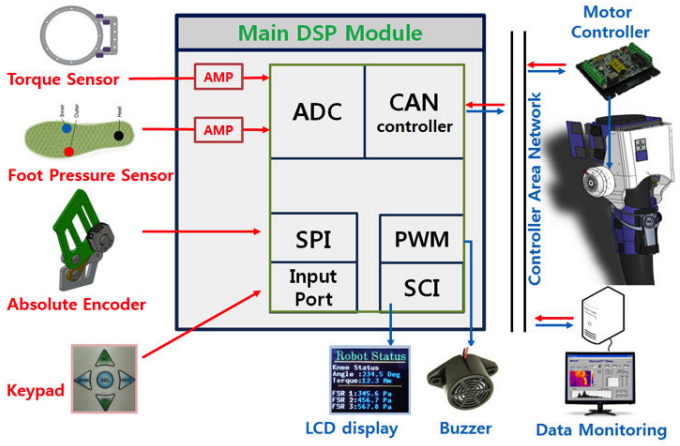


**Figure 11.** Electrical hardware architecture

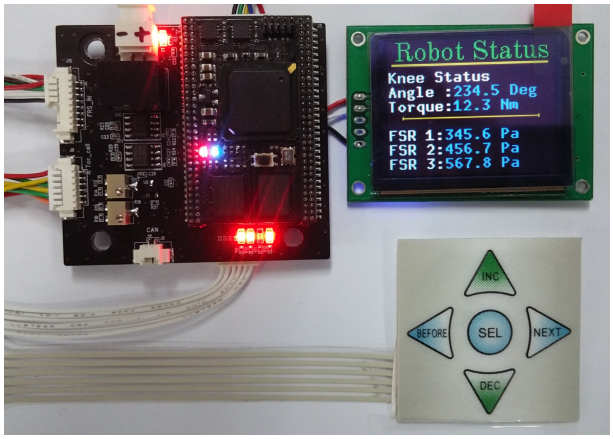


**Figure 12.** Main controller and user interfaces

## 3. Electrical Hardware and Sensor Design

### *3.1 Electrical Hardware*

The overall electrical hardware is composed of a torque sensor at the knee joint, a foot pressure sensor and an absolute encoder, as depicted in Figure 11.

For the motor controller, we used a commercialized product that has a controller area network (CAN) interface, a 20~80 KHz PWM frequency, a high continuous current output of 8 A, is lightweight, and so on. The primary digital signal processor transmits the position and torque commands to the motor controller and it includes the sensor interfaces and I/O modules (LCD, keypad, and buzzer), as illustrated in Figure 12. The LCD display shows the status (current angle, torque and FSR values) of the robot and preference settings. Using the keypad, the user can set the range of knee motion (knee angle) and enter his/her weight value for optimal control. The buzzer was used to inform the user whether the robot touched the ground safely or not.

### *3.2 Torque Sensor*

Strain gauges were used for the torque feedback. The appropriate gauge positions were determined using simulations that applied 300~400 uε strain when a 35 Nm moment was supplied at the shank (Figures 13 and 14). Furthermore, they were attached to a full bridge in order to sense the torque of the actuating module. Through the experiments, voltage values at $V_{ext}$ = 5 V and gain = 1,000 were obtained. Finally, the relationship ($T_{shank}$ = $aV_{output}$) was derived using curve fitting in the control algorithm (Figure 15).

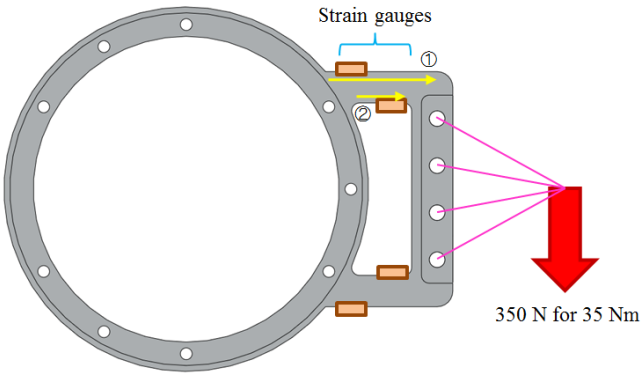


**Figure 13.** Strain gauge attachment configuration; the full bridge wiring is applied electrically

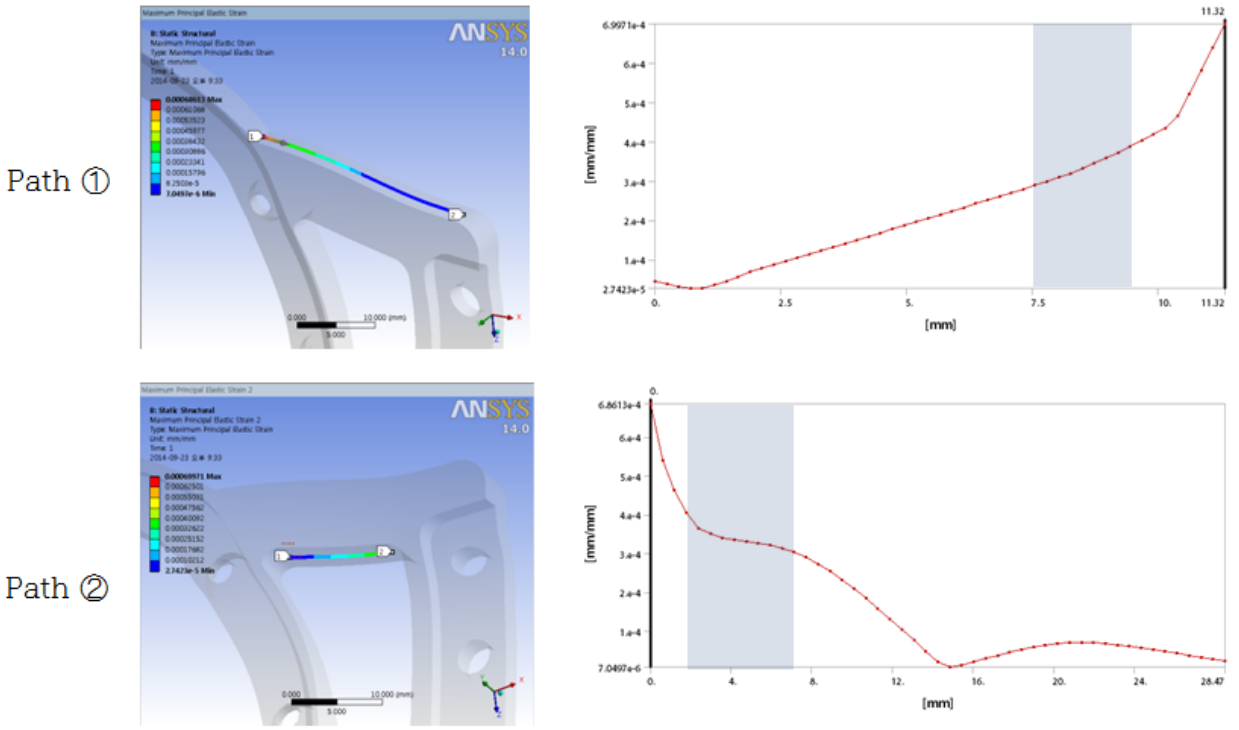


**Figure 14.** Strain variations along defined paths. The grey-shaded boxes are the range where 300~400 uε occurred.

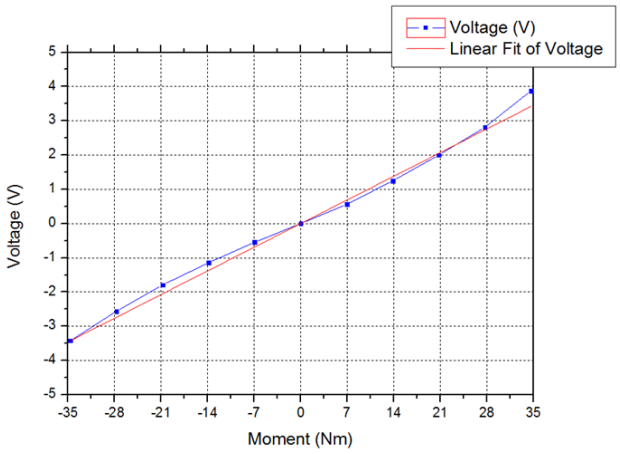


**Figure 15.** Full bridge strain gauge experiment results: the result plot is approximated to the first-order equation ($T_{shank} = 0.099V_{output}$) for the control algorithm

### *3.3 Foot Sensor*

The centre of pressure (COP) in a sole when measured during walking is important information in the control of rehabilitation and exoskeleton robots [8, 19]. Various foot sensors have been developed in previous studies. Among them, implantable foot sensors were inserted into shoes, and these have significant benefits of portability and user-friendliness; thus, they are used widely [20].

In this study, we developed a foot sensor for the exoskeleton robot. The purpose of the sensor is to obtain a reliable COP by measuring the exact load without being susceptible to the noise that can be generated from the motor and being comfortable when worn. Furthermore, the foot sensor developed in this study is used to control the exoskeleton robot, and the sensor can be inserted into a shoe.

In order to select an appropriate sensor for the foot sensor device, we experimented to measure different foot pressures. The measurements were performed using a number of experiments with a body pressure measurement system (BPMS), as depicted in Figure 16.

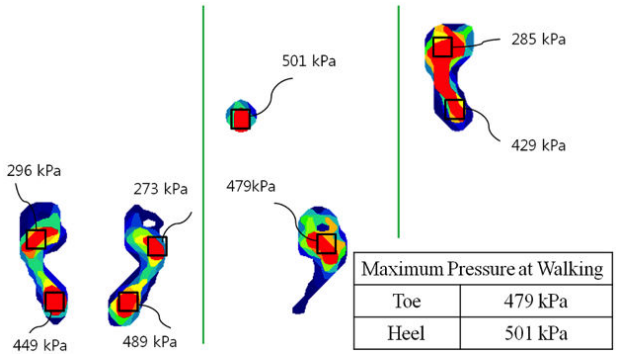


**Figure 16.** Measurement of the foot pressure using BPMS

We conducted a number of steps in the BPMS. As a result of the experiments, we selected the position of the maximum working pressure of the foot. Furthermore, the foot pressures on the front and rear parts were approximately 479 kPa and 501 kPa, respectively.

Based on the experimental results, we selected the A401 force-sensing resistor (FSR) developed by Tekscan, because it has a wide measurement range. We used the three FSRs

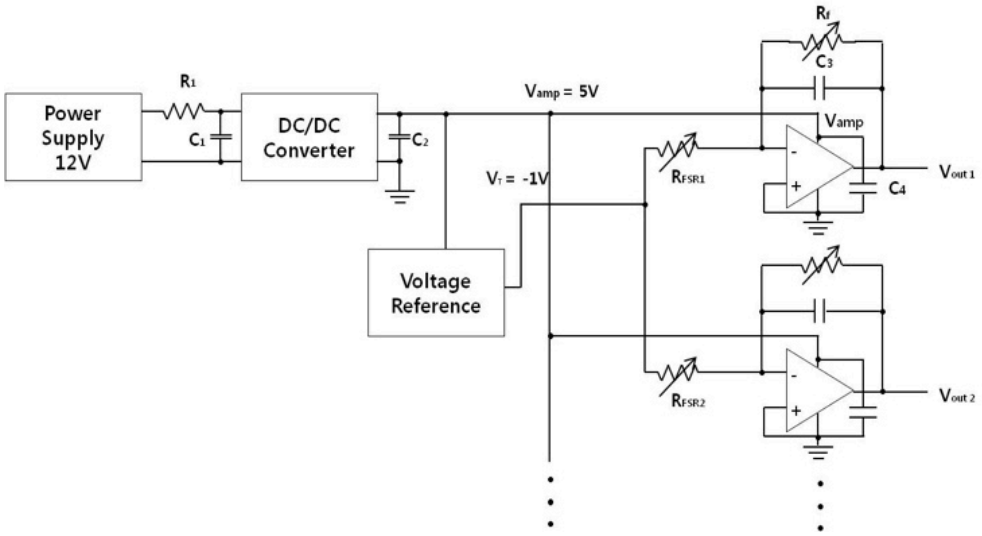


**Figure 17.** Inverted operating amplifier circuit for the FSRs

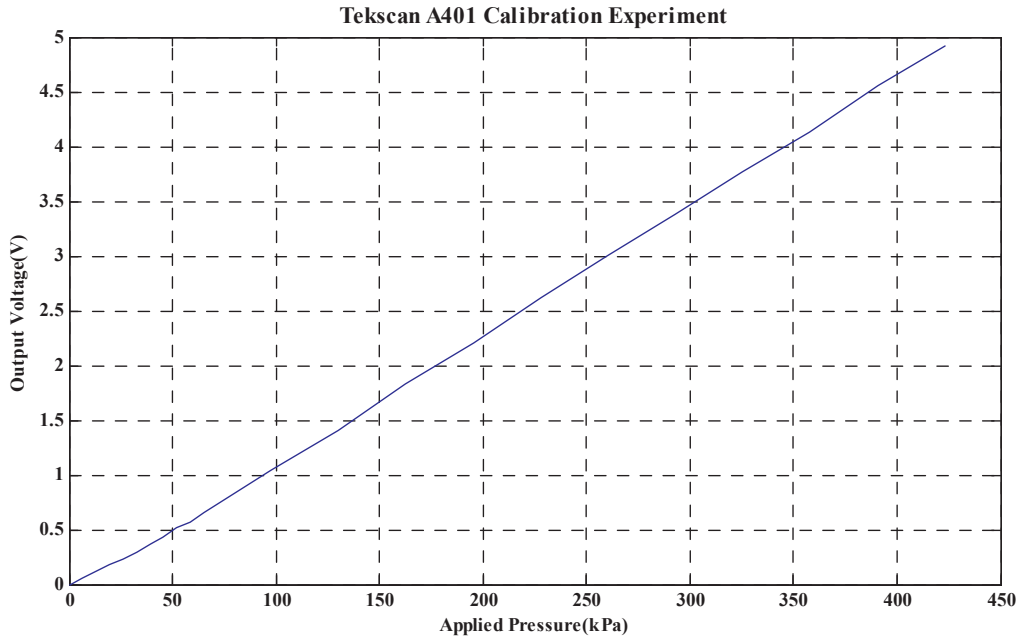


**Figure 18.** Applied pressure – output voltage plot from the calibration experiment

to measure the foot pressure efficiently, and the locations of the FSRs were determined appropriately through experiments.

Because the output voltage is non-linear, it is difficult to calibrate for non-inverting amplifier circuits. For this reason, we configured the inverted operating amplifier circuit as depicted in Figure 17, where the output voltage of the inverted operating amplifier is proportional to the absolute value of the FSR conductance and is amplified by the driving voltage (VT) and resistance (Rf) according to equation (4).

$$\left(V_{out}\right)_i = -V_T \frac{R_f}{\left(R_{FSR}\right)_i} \tag{4}$$

In order to measure the precise signals, it is important to supply the VT and supplying voltage stably. After these processes, we measured the FSR signal with respect to the various pressures, as depicted in Figure 18. The output voltage of the electrical circuit had a linear relationship to the applied pressure.

The initial foot sensor had noise at a frequency of 500 Hz, as illustrated in the upper part of Figure 19. In order to remove this noise, we designed a passive low-pass filter with a cut-off frequency of 331.74 Hz. In addition, in order to minimize the noise due to the magnetic field of the motor, a twisted pair shielded cable was used.

The COP of the wearer was calculated using equation (5) and the foot pressures were measured from the insole foot sensor.

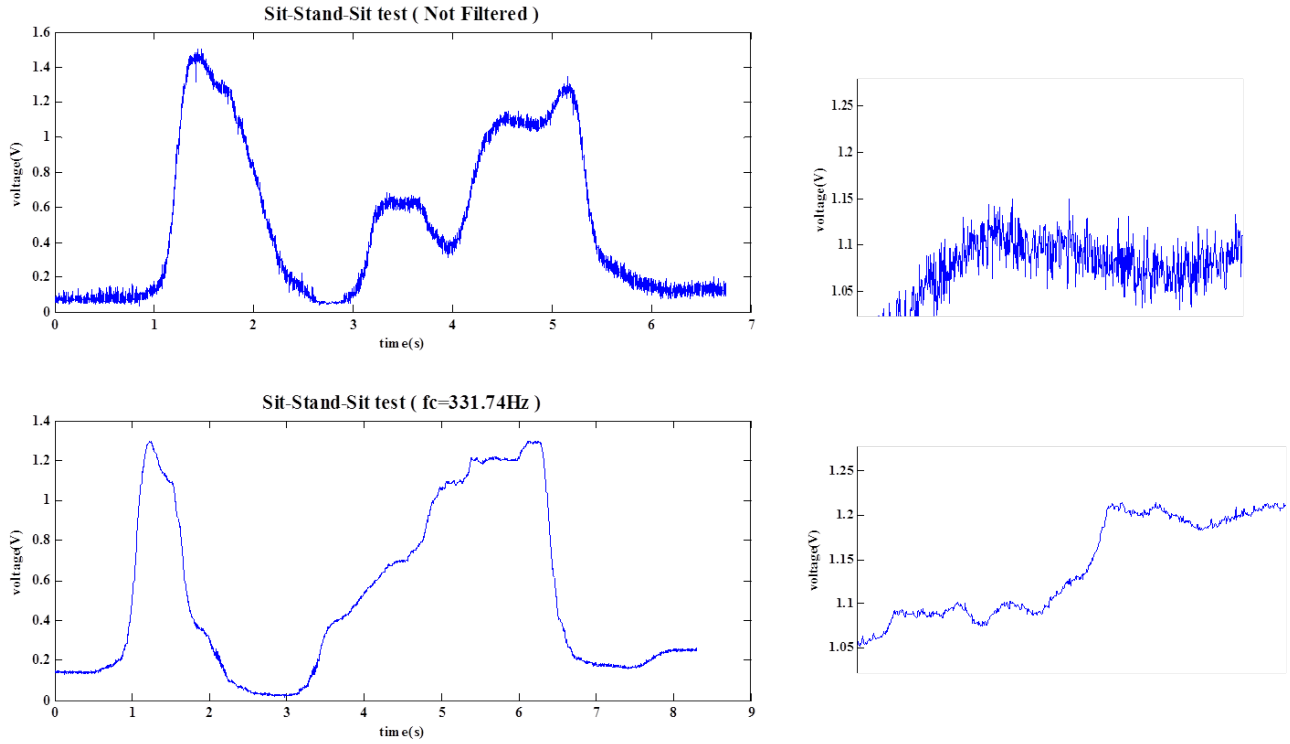


**Figure 19.** Removal of noise in the FSR sensor signal

$$GRF = \sum_{i=1}^{3} F_i,\ CoP_x = \sum_{i=1}^{3} \frac{F_i \cdot x_i}{GRF},\ CoP_y = \sum_{i=1}^{3} \frac{F_i \cdot y_i}{GRF} \quad (5)$$

The parameters of the above formula indicated by *xi* and *yi* refer to the position of the FSRs when assuming that the left and bottom sides of the heel are the origin, and the three FSR sensors were attached to appropriate locations which were determined using experiments with the BPMS (Figure 16, 20).


**Figure 20.** Insole foot pressure sensor using three FSRs

Figure 21 presents the COP calculated using the proposed system when a human wearing the foot sensor walks on normal terrain.

As a result, it was possible to measure the signal within the appropriate range and to calculate the COP.

### *3.4 System Integration*

Figure 22 presents the developed knee exoskeleton with the insole foot pressure sensor. A torque sensor was attached to the frame between the actuator module and thigh. This sensor was composed of a Wheatstone bridge with two active strain gauges and two resistors. The binding with a dial was used to connect the human and the robot. When the user turns the dial, the binding tightens the thigh and the shank. The robot was powered using an external source (24 V) or Li-Po battery.

## 4. Control Algorithm and Experiment

### *4.1 Control Algorithm*

For the basic test to verify the developed hardware and sensor system, control algorithms were developed in order to assist the normal gait, moving from sitting to standing, and moving from standing to sitting.

The Tibion PK100 is well known as a commercial exoskeleton robot that supports the knee joint [8, 9]. Its operation method is motor control by changing the gear ratio. For example, the robot decreases the gear ratio during the swing motion. However, our developed robot changes the stiffness of the actuator by software so that we can reduce

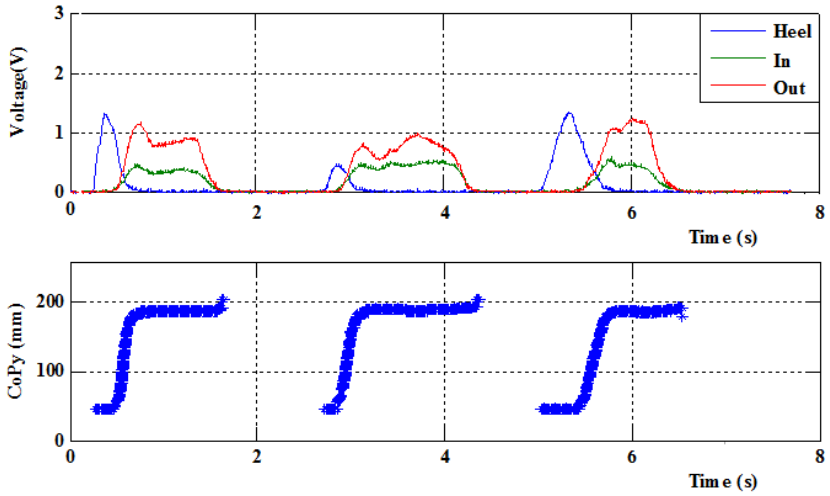


**Figure 21.** COP trajectory along the y-axis while walking three steps

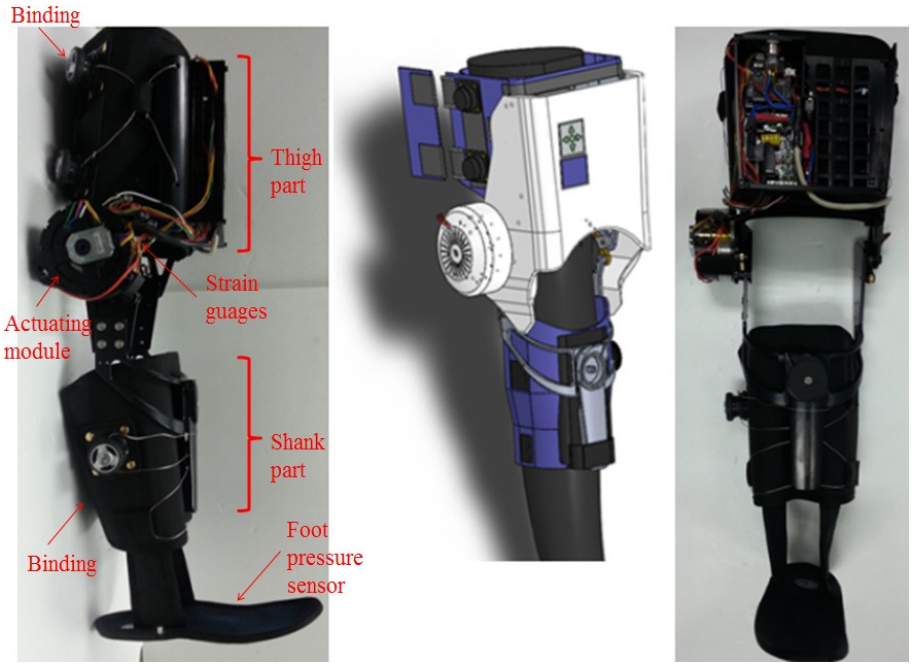


**Figure 22.** The developed knee exoskeleton robot

its weight (Tibion PK100: 3.7 kg; our robot 3.5 kg), and the compatibility of the proposed algorithm was experimentally tested with the robot.

**a.** Finite State Machine

Our control algorithm is based on an FSM, where the states are START, END, SIT, SIT2STAND, STAND, SWING and STAND2SIT, as depicted in Figure 23. Each state operates the necessary assistive knee action using an appropriate control method.

**b.** Detecting User Intention

It is important for the robot to be able to detect the user's intention. The encoder, knee torque sensor and three FSRs attached to the robot are used as trigger signals in the state transition of the FSM as well as the basic control and feedback variables in each state.

**c.** SIT-STAND-SIT Algorithm

If a person wearing the exoskeleton robot tries to stand up, the FSR signals change. Thereafter, the robot performs a SIT2STAND motion using the force control method, and the robot gives the wearer sufficient torque to stand up. After the SIT2STAND motion is completed, the position control begins maintaining the user's posture. When the user tries to bend his/her knee to sit down, the torque sensor can identify the intention and then the robot performs the STAND2SIT motion using a virtual damper control [21, 22] to prevent the user from falling by actuating the knee joint like a damper system.

**d.** Walking Algorithm

During walking, there are two states: the STAND state and the SWING state. The states are determined by the foot pressure sensors. The stand controller maintains the user's posture to prevent him/her from falling. The swing controller generates a natural motion to follow the user's knee joint motion according to his/her intention. This is an impedance control method that uses the torque data measured by the torque sensor [23]. There are many types of impedance control, and an explicit force control was applied here.

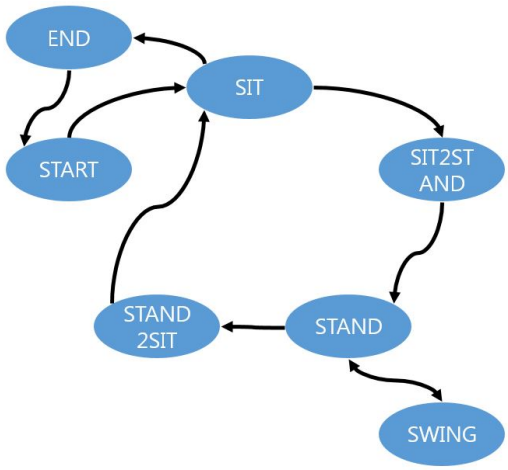


**Figure 23.** State diagram for the knee exoskeleton robot

| **Require:** |
|---|
| State – START, SIT, SIT2STAND, STAND, SWING, STAND2SIT |
| Sensor – Encoder [degree, 0~ -120°], 3 FSRs [kPa], |
| Torque sensor [Nm] |
| FSRs – FSR_Rear, FSR_FootInside, FSR_FootOutside, |
| FSR_SUM |
| Threshold: Boundary value of state |
| // first state: START |
| **if** State==START && encoder<threshold_1 |
| State = SIT |
| Impedance control starts. |
| **end if** |
| **if** State==SIT && FSR_SUM > threshold_2 |
| State = SIT2STAND |
| Move to -10° //by current control |
| **end if** |
| **if** State==SIT2STAND && encoder > =threshold_3 |
| State = STAND |
| Maintain a motor position //by position control |
| **end if** |
| **Require:** |
| **if** State==STAND && FSR_SUM<=threshold_4 |
| State = SWING |
| Impedance control starts. |
| **end if** |
| **if** State==SWING && FSR_SUM > threshold_5 |
| State = STAND |
| Position control starts. |
| **end if** |
| **if** State==STAND && torque<threshold_6 |
| State = STAND2SIT |
| Input current = constant current + virtual damper |
| **end if** |
| **if** State==STAND2SIT && FSR_SUM<=threshold_7 |
| State = SIT |
| **end if** |

**Table 1.** Control algorithm pseudocode

*4.2 Experiment*

In order to identify the user's intentions related to the threshold values, basic test experiments of standing, walking and sitting motions were performed with healthy subjects wearing the knee exoskeleton and insole pressure sensors without applying a control method. The experimental results demonstrated that the user's standing and sitting postures were not all the same. Some people put their weight on the fore part of the foot during standing and sitting. In contrast, other people put their weight near the rear foot. Therefore, the sum of the three pressure sensors (FSRs) was selected as a threshold in order to apply the knee exoskeleton to most users.

In order to validate the designed hardware and basic software system, experiments on able-bodied subjects wearing the developed knee exoskeleton while standing, sitting and walking were performed. It should be noted that tuning of the threshold values is required because the users' weights and required torque levels for increasing comfort differ. Figure 24 illustrates the knee angle measured from the encoder, the knee torque and the foot pressure signal on the FSRs when a healthy person weighing 75 kg wore the knee exoskeleton and undertook the following motions: standing up from a chair, marching in place for four steps, and sitting down on the chair. The variable fsr_sum indicates the sum of the three FSRs (fsr_rear, fsr_inside, and fsr_outside) on the sole.

First, when the wearer sitting on a chair tried to stand up, the weight centre moved from the chair to the foot and the resulting fsr_sum signal increased. When the fsr_sum was over a specified threshold pressure (15 kPa), the SIT state changed to SIT2STAND. In this figure, the instance of this state transition is at approximately 4 s. In the SIT2STAND

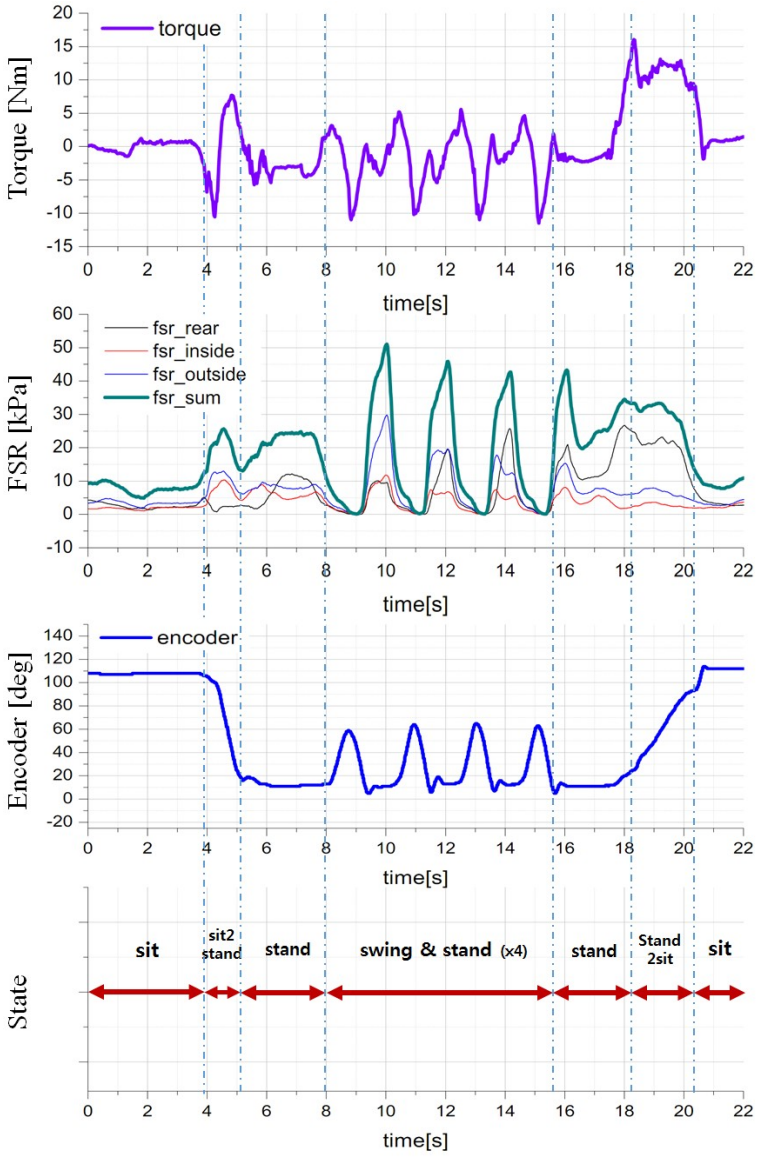


**Figure 24.** Knee torque, foot pressure and knee angle during the SIT2STAND, SWING, STAND and STAND2SIT states

state, the knee joint angle is extended until the knee angle reaches a threshold angle. In this experiment, the threshold angle was 20 degrees and the state changed to the STAND state when the knee angle reached the threshold angle in the SIT2STAND state. During the STAND state, the state was changed to the swing state when fsr_sum decreased to less than 12 kPa. Meanwhile, the SWING state was changed to the STAND state when fsr_sum was more than 20 kPa. The periodic transitions between the STAND and SWING states were repeated while marching in place for four steps. Finally, when the wearer tried to sit down, the knee torque sensor signal increased. When the torque increased over the torque threshold of 15 Nm in the STAND state, it was changed to the STAND2SIT state. While sitting down, the knee was flexed, the FSR signals decreased and the encoder signal increased. If fsr_sum was less than 15 kPa and the encoder degree was more than 70 degrees, the STAND2SIT state was changed to the SIT state.

## 5. Conclusion and Future Work

In this paper, a knee-assistive exoskeleton device for hemiplegic patients was designed. The device is a stand-alone system that includes a microprocessor, a battery, an LCD display, a buzzer and a user's button inputs; furthermore, it is a portable system that only weighs 3.5 kg. The hardware architecture was designed for rapid future development. For example, it can be controlled using a controller area network (CAN) on a PC or an embedded microprocessor. It can also provide real-time sensing data and the inner states of the program via CAN. The ergonomic aspects were considered, including the polycentric joint with a four-bar linkage, and analyses were performed in order to estimate its output torque and speed. In order to determine the user's intention, an insole foot pressure sensor and interface electronics were designed. The sensors were constructed using thin FSRs, which can estimate the COP with reasonable accuracy. The torque sensor is

another sensor that detects the user's intention. The strain gauge attached to the link frame enabled the lightweight design. The strain gauge was used to measure the torque at the knee joint, and eventually it was used in the force control during the SWING and STAND2SIT states. The absolute encoder also provided convenience to avoid calibrating the initial position and fail safety function in addition to the incremental encoder. The basic algorithms were designed based on an FSM, and through the experiments for moving from sitting to standing, walking, and moving from standing to sitting control, we verified the proposed design and algorithm as the first step of development.

A brief comparison of our knee exoskeleton and other studies is listed on Table 2. The weight of our system involves the weight of the actuator, the brace, electronics, a battery, a user interface (keypad, LCD display, buzzer). Most of all, the polycentric joint could provide more comfortable wearability to the wearer and maintain the binding force between wearer and robot.

| Knee exoskeleton | Weight | Range of motion | Battery-powered | Knee axis |
|---|---|---|---|---|
| RoboKnee [24] | 3 kg (without battery) | - | O | Single-axis |
| EMG-Knee [25] | 5 kg (without battery) | 120 deg | X | Single-axis |
| Quasi-Passive Knee [26] | 2.5 kg | 97 deg | O | Single-axis |
| Bionic Leg [8, 27] | 3.7 kg | 120 deg | O | Single-axis |
| Our system | 3.5 kg | 120 deg | O | Polycentric |

**Table 2.** Comparison of our system with other studies

In the future, we will apply the designed assistive knee exoskeleton to hemiplegic patients using more enhanced algorithms, and we will continue to improve the system with regard to patients and therapists. In addition, we will develop algorithms for supporting daily life for patients, such as climbing up and down stairs as well as flat surfaces; we will also extend our application to rehabilitation training using a more interesting game interface.

## 6. Acknowledgements

This study was supported by a grant from the Translational Research Center for Rehabilitation Robots, Korea National Rehabilitation Center, Ministry of Health and Welfare, Republic of Korea.

This study was also supported by a grant from the Human Resources Development Program (No. 20134010200580) of the Korea Institute of Energy Technology Evaluation and Planning (KETEP), funded by the Ministry of Trade, Industry and Energy, Republic of Korea.

## 7. References

[1] ReWalk – More than Walking [Internet]. (2014) [updated 2014; cited 02 Dec 2014]. Available from: http://www.rewalk.com. Accessed on 23 Dec 2014.

[2] K. A. Strausser, T. A. Swift, et al. (2011) Mobile Exoskeleton for Spinal Cord Injury: Development and Testing. ASME 2011 Dynamic Systems and Control Conference and Bath/ASME Symposium on Fluid Power and Motion Control (DSCC2011). 2011 Oct 31-Nov 2; Arlington, Virginia, USA. ASME. pp. 419-425.

[3] K. A. Strausser and H. Kazerooni (2011) The Development and Testing of a Human Machine Interface for a Mobile Medical Exoskeleton. 2011 IEEE/RSJ International Conference on Intelligent Robots and Systems (IROS). 2011 Sep 25-30; San Francisco, CA. IEEE. pp. 4911-6.

[4] H. Kawainot, O. S. Lee, et al. (2003) Power Assist Method for HAL-3 using EMG-based Feedback Controller. 2003 IEEE International Conference on Systems, Man and Cybernetics. 2003 Oct 5-8; IEEE. pp. 1648-53.

[5] C. Fleischer, C. Reinicke, et al. (2005) Predicting the Intended Motion with EMG Signals for an Exoskeleton Orthosis Controller. 2005 IEEE/RSJ International Conference on Intelligent Robot and Systems (IROS). 2005 Aug 2-6; IEEE. pp. 2029-34.

[6] C. J. Walsh, K. Pasch, et al. (2006) An Autonomous, Underactuated Exoskeleton for Load-Carrying Augmentation. 2006 IEEE/RSJ International Conference on Intelligent Robots and Systems (IROS). 2006 Oct 9-15; Beijing, China. IEEE. pp. 1410–5.

[7] C. J. Walsh, K. Endo, H. Herr (2007) Quasi-passive Leg Exoskeleton for Load-carrying Augmentation. International Journal of Humanoid Robotics. 4(3): 487–506.

[8] R. W. Horst (2009) A Bio-robotic Leg Orthosis for Rehabilitation and Mobility Enhancement. 2009 Annual International Conference of the IEEE Engineering in Medicine and Biology Society (EMBC2009). 2009 Sep 3-6; Minneapolis, MN. IEEE. pp. 5030–3.

[9] R. W. Horst (2006) FlexCVA: A Continuously Variable Actuator for Active Orthotics. 2006 28th Annual International Conference of the IEEE Engineering in Medicine and Biology Society (EMBS06). 2006 Aug 30- Sep 3; New York City, USA. IEEE. pp. 2425-8.

[10] P. N. Smith, K. M. Refshauge, J. M. Scarvell (2003) Development of the Concepts of Knee Kinematics. Archives of Physical Medicine and Rehabilitation. 84(12): 1895-1902.

[11] T. Fitzsimons, Knee Disarticulation a Whirlwind Tour [Internet]. 2008 [updated 27 June; cited 2 December] Available from: http:// www.geoci-

ties.ws/nswpar/Knee_Disarticulation.pdf. Accessed on 24 Nov 2014.

[12] M. P. Greene (1983) Four Bar Linkage Knee Analysis. Orthotics and Prosthetics. 37(1): 15-24.

[13] S. A. Gard, D. S. Childress, et al. (1996) The Influence of Four Bar Linkage Knees on Prosthetic Swing Phase Floor Clearance. Journal of Prosthetics and Orthotics. 8(2): 34-40.

[14] M. R. Tucker, A. Moser, et al. (2013) Design of a Wearable Perturbator for Human Knee Impedance Estimation during Gait. In: IEEE, editor. 2013 IEEE International Conference on Rehabilitation Robotics (ICORR). 2013 Jun 24-26; Bellevue, Washington. pp. 1-6.

[15] B. Celebi, M. Yalcin, et al. (2013) Assist On-knee: A Self-aligning Knee Exoskeleton. In: IEEE, editor. 2013 IEEE/RSJ International Conference on Intelligent Robots and Systems (IROS 2013). 2013 Nov 3-8; Tokyo, Japan. pp. 996-1002.

[16] K. Manal, I. McClay, et al. (2002) Knee Moment Profiles during Walking: Errors due to Soft Tissue Movement of the Shank and the Influence of the Reference Coordinate System. Gait and Posture. 15(1): 10-17.

[17] M. P. Kadaba, H. K. Ramakrishnan, et al. (1990), Measurement of Lower Extremity Kinematics during Level Walking. Journal of Orthopaedic Research. 8(3): 383-392.

[18] R. L. Norton (2004) DESIGN OF MACHINERY: An Introduction to the Synthesis and Analysis of Mechanisms and Machines (3rd edition), New York: McGraw-Hill Education. pp. 174-178.

[19] A. L. Randolph, M. Nelson, et al. (2000) Reliability of Measurements of Pressures Applied on the Foot During Walking by a Computerized Insole Sensor System. Archive of Physical Medicine and Rehabilitation. 81(5): 573-578.

[20] A. M. Howel, T. Kobayashi, et al. (2013) Kinetic Gait Analysis Using a Low-cost Insole. IEEE Transactions on Biomedical Engineering. 60(12): 3284-3290.

[21] J. H. Kim, J. Y. Kim and J. H. Oh (2008) Adjustment of Home Posture of Biped Humanoid Robot using Sensory Feedback Control. Journal of Intelligent & Robotic Systems. 51(4), 421-438.

[22] J. H. Kim, J. Y. Kim and J. H. Oh (2011) Adaptive Walking Pattern Generation and Balance Control of the Passenger-Carrying Biped Robot. HUBO FX-1, for Variable Passenger Weights. Advanced Robotics. 30(4):427-443.

[23] R. Volpe and P. Khosla (1993) A Theoretical and Experimental Investigation of Explicit Force Control Strategies for Manipulators. IEEE Transactions on Automatic Control. 38(11): 1634-1650.

[24] J. E. Pratt, B. T. Krupp, J. Christopher (2004) The RoboKnee: An Exoskeleton for Enhancing Strength and Endurance During Walking. Proceedings of the IEEE International Conference on Robotics and Automation New Orleans, LA, pp. 2430-5.

[25] C. Fleischer and G. Hommel (2008) A Human–Exoskeleton Interface Utilizing Electromyography. IEEE Transactions on Robotics. 24(4): 872-882.

[26] A. M. Dollar and H. Herr. (2008) Design of a Quasi-passive Knee Exoskeleton to Assist Running. IEEE/RSJ International Conference on Intelligent Robots and Systems, Nice, France. pp. 747-54.

[27] C. K. Wong, L. Bishop and J. Stein (2012) A Wearable Robotic Knee Orthosis for Gait Training: a Case-Series of Hemiparetic Stroke Survivors. Prosthetics and Orthotics International. 36(1): 113-120.